Supporting Information

Nonproductive Binding Modes as a Prominent Feature of $A\beta_{40}$ Fiber Elongation: Insights from Molecular Dynamics Simulation

Rajiv K Kar,[1] Jeffrey R Brender,[2] Anirban Ghosh,[1] Anirban Bhunia[1,*]

[1]Department of Biophysics, Bose Institute, P-1/12 CIT Scheme VII (M), Kolkata 700054, India;
[2]Radiation Biology Branch, National Institutes of Health, Bethesda, MD 20814, USA

*** To whom correspondence should be addressed:**

Dr. Anirban Bhunia

Email: anirbanbhunia@gmail.com / bhunia@jcbose.ac.in

Tel: +91-33-2569 3336

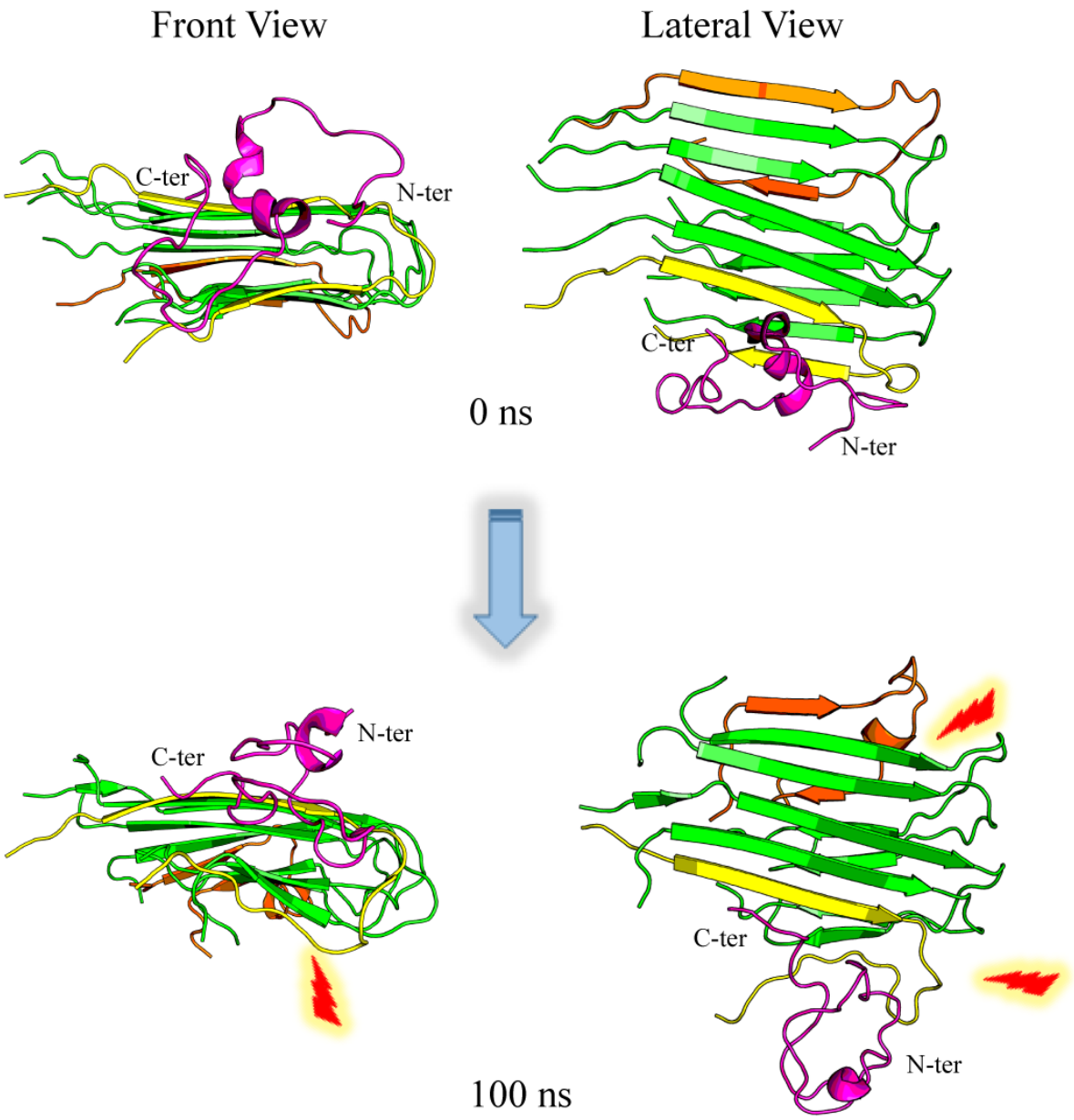

Figure S1: Step-wise changes: Fiber-monomer contacts Analysis of the molecular fluctuations in the amyloid fiber in the presence of $A\beta_{1\text{-}40}$ from 0 ns to 100 ns. The incoming $A\beta_{1\text{-}40}$ monomer docked to the amyloid fiber is shown in pink color. The fragment to which $A\beta_{1\text{-}40}$ is docked (near-fragment) is shown in yellow and the extreme end (far-fragment) is shown in orange. Significant changes in the secondary structure of near and far-fragment are shown with red highlights.

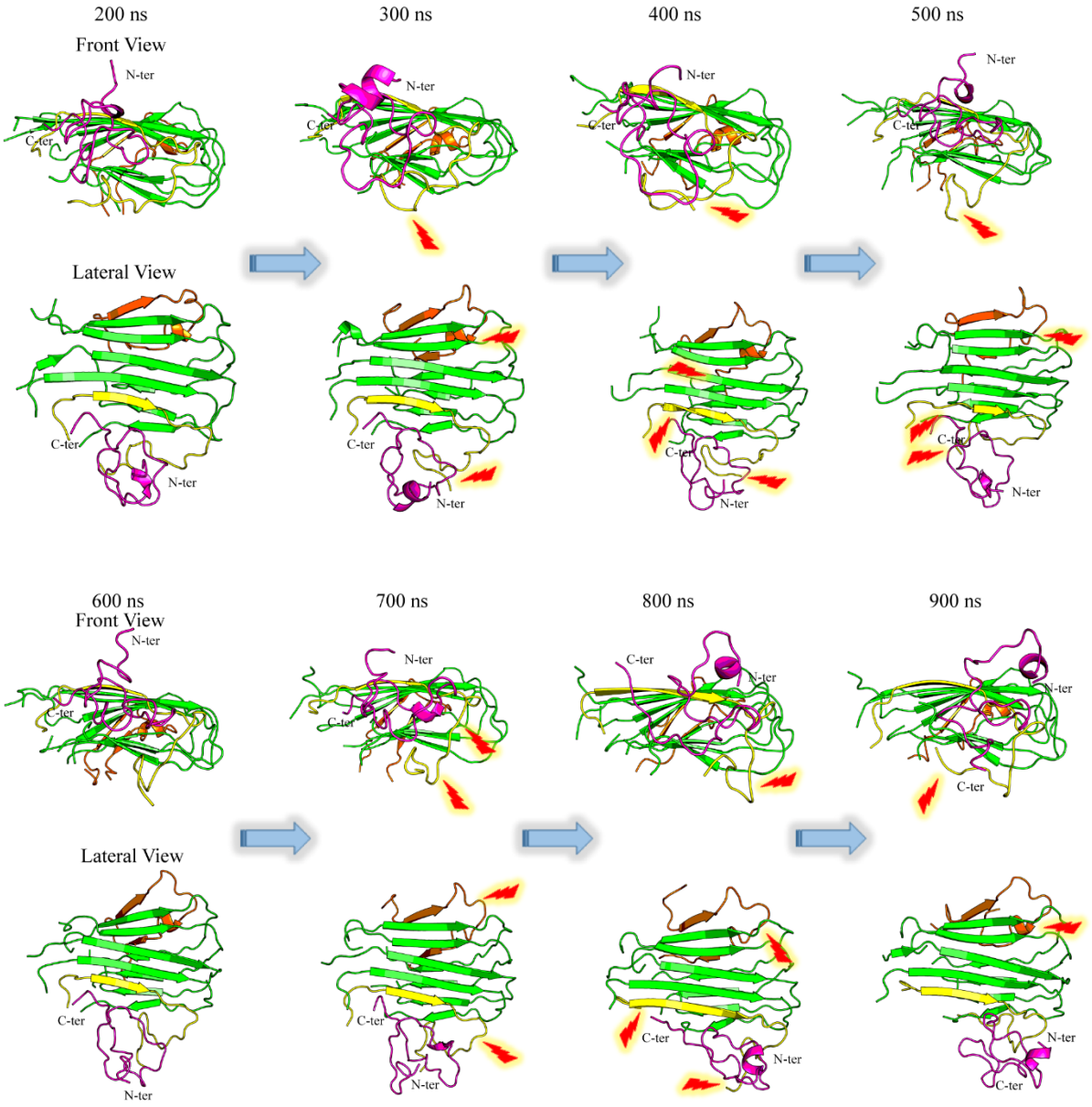

Figure S2: Analysis of the molecular fluctuations in the amyloid fibrillar structure in presence of $A\beta_{1\text{-}40}$ from 200 ns to 900 ns. The incoming $A\beta_{1\text{-}40}$ monomer docked to the amyloid fiber is shown in pink color. The fragment to which $A\beta_{1\text{-}40}$ is docked (near-fragment) is shown in yellow and the extreme end (far-fragment) is shown in orange. Significant changes in the secondary structure of near and far-fragment are shown with red highlights.

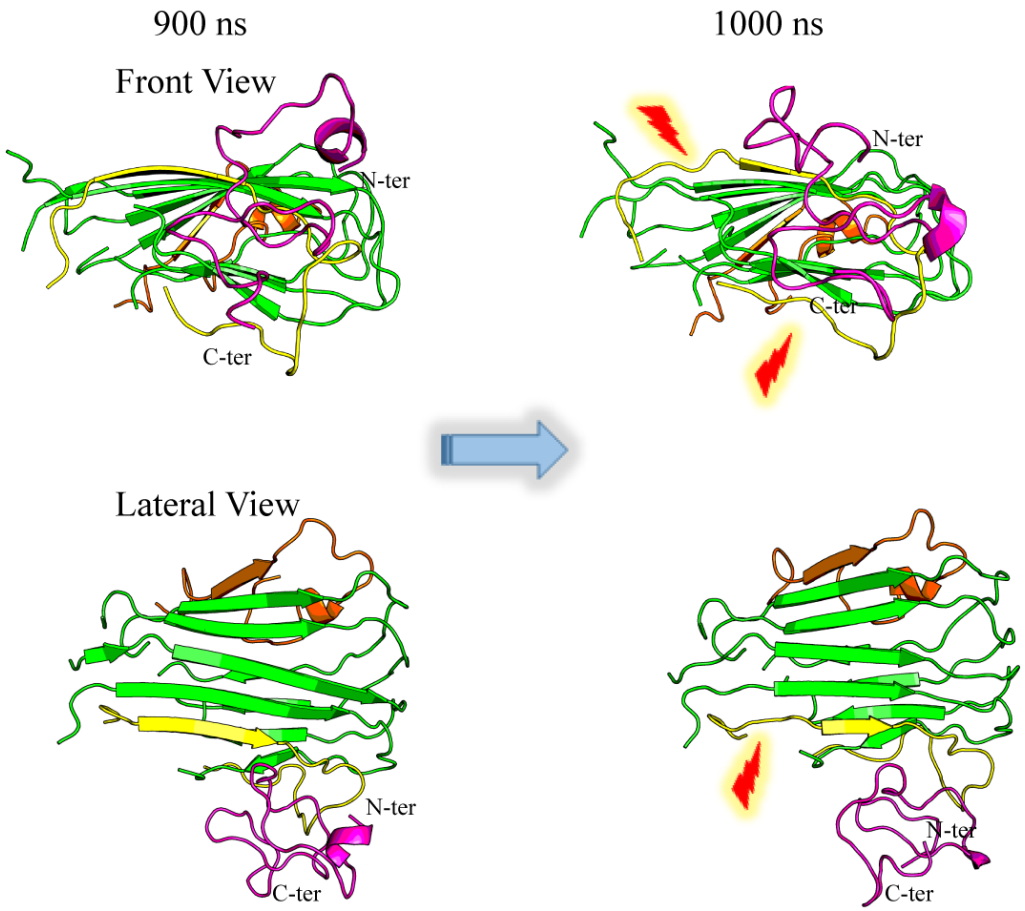

Figure S3: Analysis of the molecular fluctuations in the amyloid fibrillar structure in presence of $A\beta_{1\text{-}40}$ from 900 ns to 1000 ns. The incoming $A\beta_{1\text{-}40}$ monomer docked to the amyloid fiber is shown in pink color. The fragment to which $A\beta_{1\text{-}40}$ is docked (near-fragment) is shown in yellow and the extreme end (far-fragment) is shown in orange. Significant changes in the secondary structure of near and far-fragment are shown with red highlights.

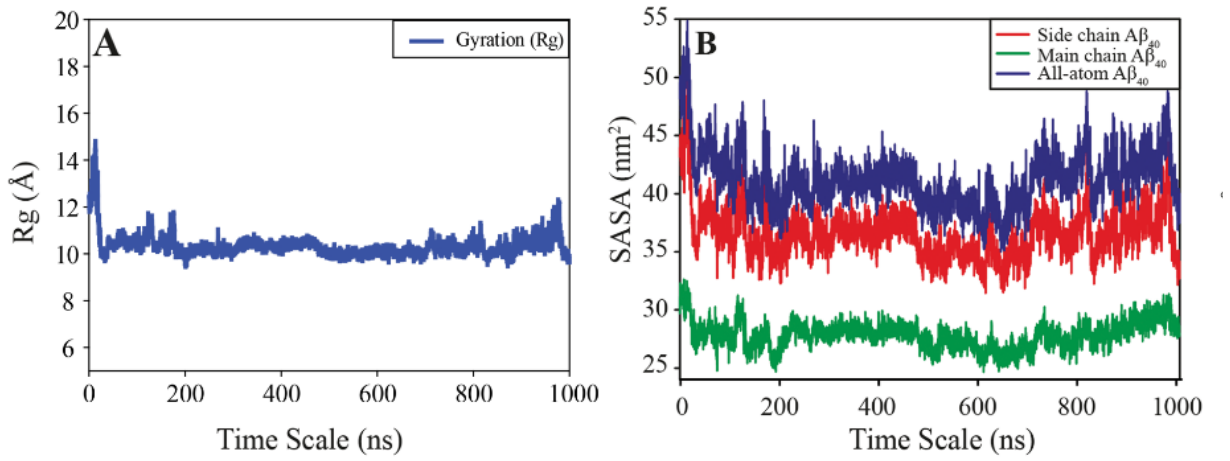

Figure S4: (A) Plot of the radius of gyration (Rg) of the monomer from the MD simulation. (B) Plot of the change in solvent accessible surface area as a function of time

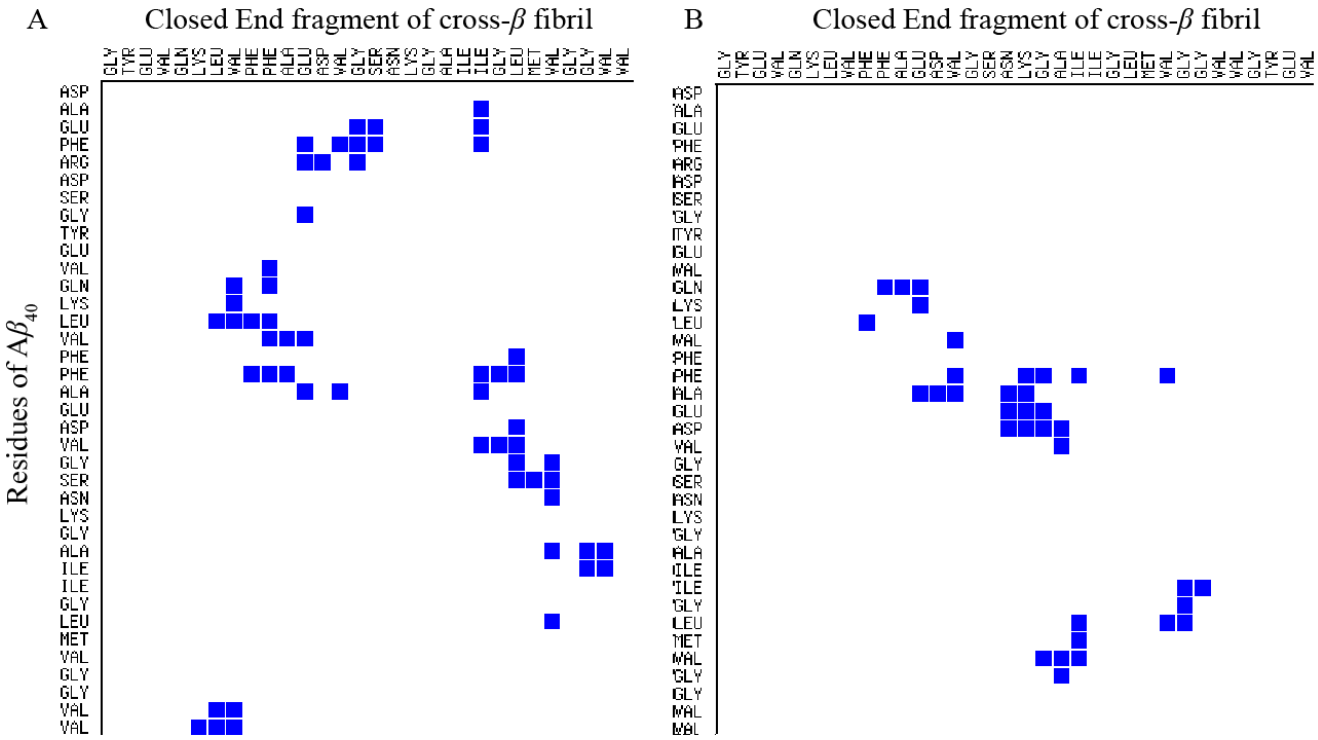

Figure S5: Contact map analysis between the fiber and monomer of complexed $A\beta_{1\text{-}40}$ at **(A)** the start of the simulation (0 ns) and **(B)** end of the simulation (1000 ns). The plot was computed using Contact Map Analysis server (ligin.weizmann.ac.il/cma/).

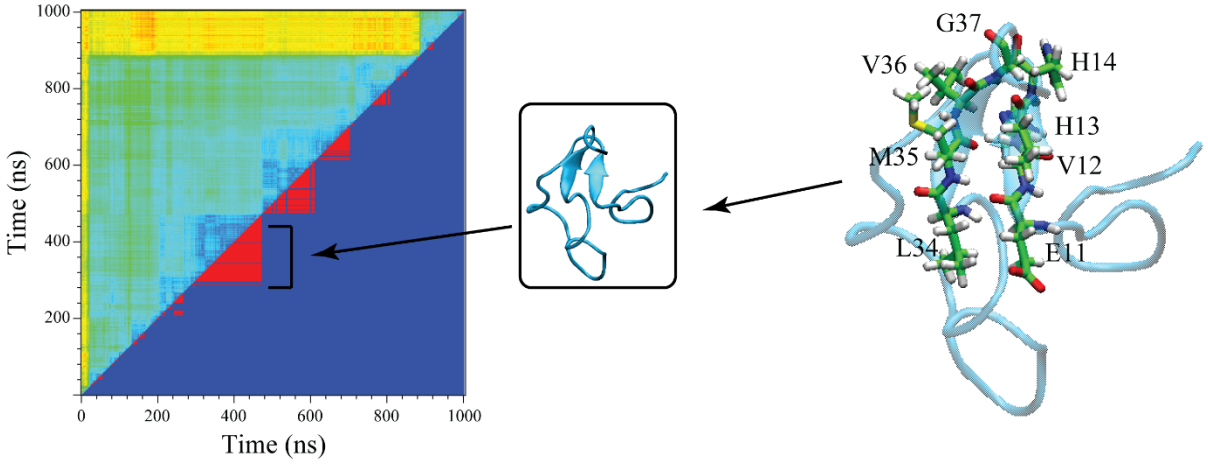

Figure S6: Representative structure from the largest cluster which appears between 300-500 ns. Residues that represent β-sheet secondary structure are shown in extreme right panel represented as sticks. The lower half triangle represents the cluster size (red).

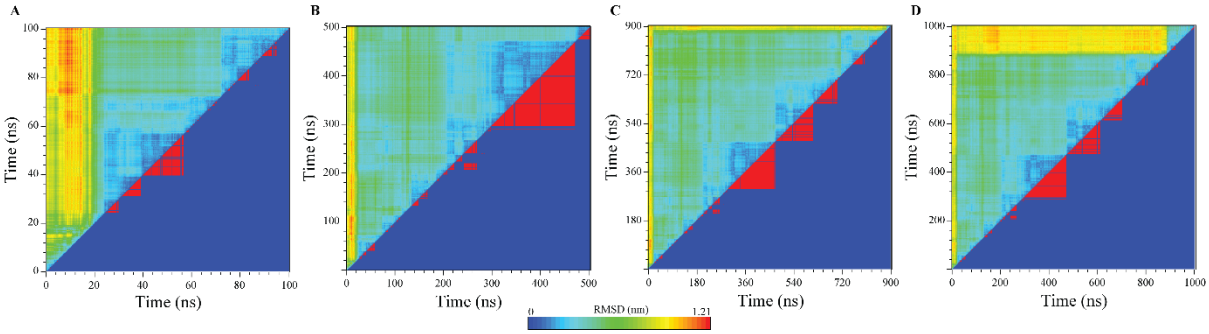

Figure S7: Cluster index based on pairwise RMSD plot for $A\beta_{1\text{-}40}$ conformations, analysed for **(A)** 0 ns – 100 ns, **(B)** 500 ns, **(C)** 900 ns, **(D)** 1000 ns. The RMSD cut-off ranges from 0 to 1.21 Å (red to blue contours). The lower half triangle represents the cluster size (red).

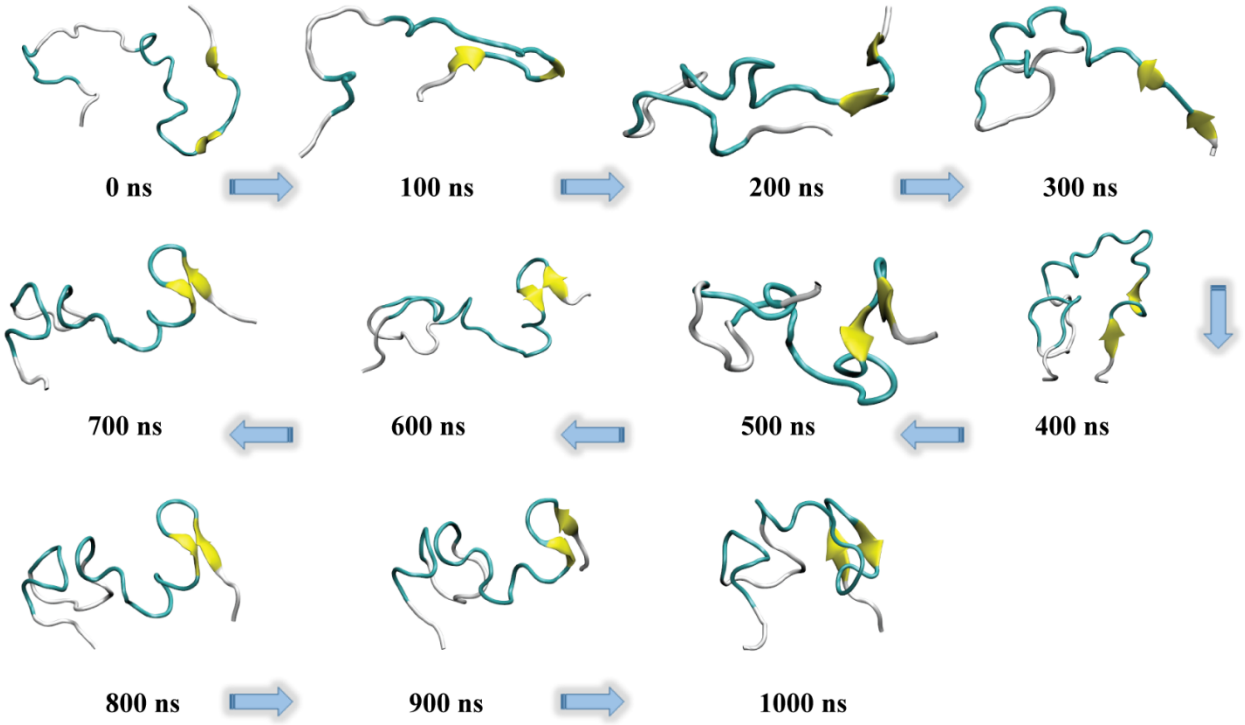

Figure S8: Snapshot representation of the conformational changes of $A\beta_{1-40}$ collected from the control simulation of monomer (without presence of amyloid fiber) in explicit solvent condition.

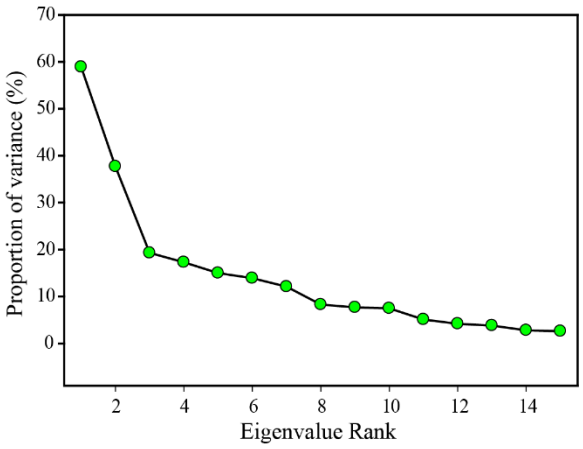

Figure S9: Scree plot showing that 81% of the collective variance in RMSD are explained by the first two principal components.

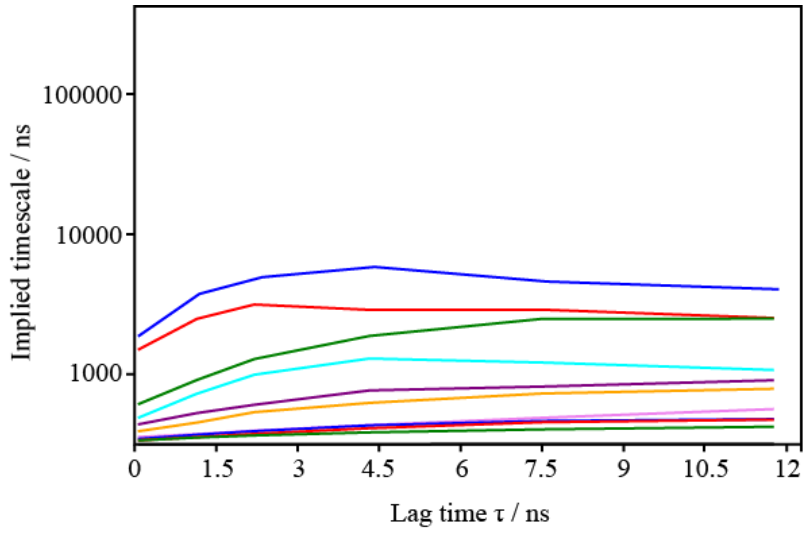

Figure S10: Implied relaxation time scale of the MSM constructed by the *k*-means algorithm constructed with 200 centers.

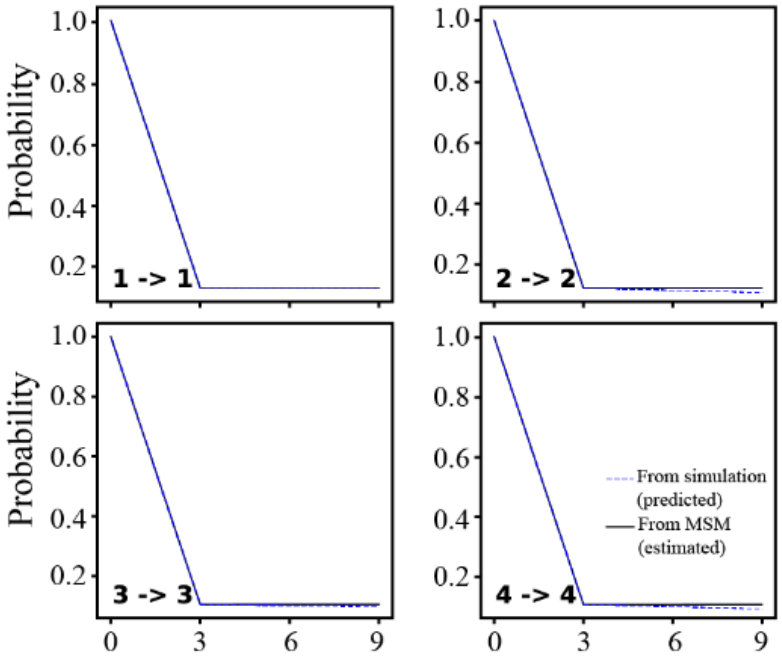

Figure S11: Results of the Chapman-Kolmogorov tests for the MSM at lag τ = 3ns.